THE JOURNAL OF PHYSICAL CHEMISTRY Letters

pubs.acs.org/JPCL

Letter

Relative Role of Physical Mechanisms on Complex Biodamage Induced by Carbon Irradiation

Simone Taioli,* Paolo E. Trevisanutto, Pablo de Vera, Stefano Simonucci, Isabel Abril, Rafael Garcia-Molina, and Maurizio Dapor*

Cite This: J. Phys. Chem. Lett. 2021, 12, 487−493

Read Online

ACCESS | Metrics & More | Article Recommendations | Supporting Information

ABSTRACT: The effective use of swift ion beams in cancer treatment (known as hadrontherapy) as well as appropriate protection in manned space missions rely on the accurate understanding of the energy delivery to cells that damages their genetic information. The key ingredient characterizing the response of a medium to the perturbation induced by charged particles is its electronic excitation spectrum. By using linear-response time-dependent density functional theory, we obtained the energy and momentum transfer excitation spectrum (the energy-loss function, ELF) of liquid water (the main constituent of biological tissues), which was in excellent agreement with experimental data. The inelastic scattering cross sections obtained from this ELF, together with the elastic scattering cross sections derived by considering the condensed phase nature of the medium, were used to perform accurate Monte Carlo simulations of the energy deposited by swift carbon ions in liquid water and carried away by the generated secondary electrons, producing inelastic events such as ionization, excitation, and dissociative electron attachment (DEA). The latter are strongly correlated with cellular death, which is scored in sensitive volumes with the size of two DNA convolutions. The sizes of the clusters of damaging events for a wide range of carbon-ion energies, from those relevant to hadrontherapy up to those for cosmic radiation, predict with unprecedented statistical accuracy the nature and relative magnitude of the main inelastic processes contributing to radiation biodamage, confirming that ionization accounts for the vast majority of complex damage. DEA, typically regarded as a very relevant biodamage mechanism, surprisingly plays a minor role in carbon-ion induced clusters of harmful events.

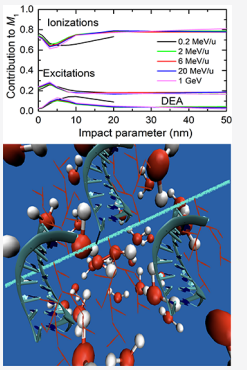

The interaction of swift ions with matter is used to probe its structure, characterize and modify materials properties, or design microdevices.[1] Energetic ion beams have also found an application in treating cancer (hadrontherapy) owing to their peculiar energy delivery to the target material, which is characterized by a depth-dose profile with a sharp peak (a so-called Bragg peak) at the end of their range where they produce severe cell damage while sparing both traversed and deeper-located healthy tissues.[2−4] The higher spatial resolution of the dose delivered by ion beams as compared to that of conventional radiation (photons and electrons) is not their only advantage. The capacity of high linear-energy-transfer (LET) ions, such as carbon ions, to produce complex DNA lesions that eventually lead to cell killing is very promising for developing more effective oncological treatments[5,6] when radiation damage to the surrounding normal tissue could be dangerous or even deadly.[7]

On the other hand, highly energetic ions with a high atomic number are also abundant in cosmic radiation. This fact poses risks to the safety of humans and devices onboard space stations, representing a serious challenge for space exploration.[8,9] Even the required coherence in quantum computers can be destroyed by cosmic rays.[10]

Achieving optimal results for selective cell destruction requires an understanding of the fundamental processes that produce most harmful lesions occurring at the cellular level. Among these, the clustering of the sugar−phosphate strand and base pair breaks in the DNA structure are mostly lethal in terms of cell survival.[11−13] Such clustered DNA lesions might be induced by several physical and chemical mechanisms.[14,15] Although indirect chemical effects can account for a large fraction of the biodamage,[16] their contributions are below 50% for high LET ions, such as carbon around the Bragg peak region.[17] As for the direct physical events, these are mainly produced by the secondary electrons abundantly generated by the incident ions. In particular, the latter can induce electronic excitations and ionizations as well as dissociative electron attachment (DEA) at energies of a few electronvolts, leading to molecular fragmentation. Since most of the electrons are ejected with energies below 50 eV, DEA has been regarded as especially relevant to biodamage.[18]

In contrast, current physical approaches to measure clustered inelastic events in targets with a DNA size, referred to as nanodosimetry,[19,20] are based on the exclusive measure-

Received: October 28, 2020
Accepted: December 10, 2020
Published: December 29, 2020

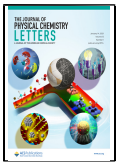

https://doi.org/10.1021/acs.jpclett.0c03250
J. Phys. Chem. Lett. 2021, 12, 487−493

ment of ionizing collisions (in gas-phase detectors, which cannot asses the role of indirect chemical events). In this context, it is crucial to precisely determine the relative contribution to clustered DNA damage for carbon ions due to the different direct interaction mechanisms. This problem can be carefully addressed either analytically, such as within the multiscale approach to the physics of radiation damage with ions,[21−23] or numerically by means of track-structure Monte Carlo (MC) simulations provided that reliable cross sections of the different interaction mechanisms with the target medium are used.[2] Typically, radiation transport is studied in liquid water, which is conventionally considered a good proxy for biological tissue due to being its main constituent.

In this work we accurately describe the liquid water electronic excitation spectrum from first-principles and simulate in detail, with remarkably high statistics, the processes occurring around the swift carbon-ion track. The relative roles of ionizations, dissociative electronic excitations, and DEA in regard to the clustering of damaging events in the medium are quantified for the first time from typical ion energies around the Bragg peak, which are useful in hadrontherapy, to cosmic ray energies, which are relevant to space missions.

The interaction of charged particles through a medium depends mainly on its electronic excitation spectrum encoded in the energy loss function ELF($\hbar k$, E),[24,25] where $\hbar k$ and E are the momentum and energy transfer, respectively. The ELF, conveniently weighted and integrated, provides the probabilities for the most important inelastic scattering processes occurring at the passage of charged particles inside a condensed medium.[2] Liquid water is the most abundant constituent of living beings; thus, a great deal of effort has been expended to obtain its ELF over the Bethe surface ($\hbar k$, E). Unfortunately, this quantity is only known experimentally for a limited range of excitation energies E and a finite set of momentum transfers $\hbar k$.[26−28] This lack of data hinders the study of energetic particles moving through biological media.

Theoretical estimates could fill the gap of the required data. However, *ab initio* computations, being mostly carried out for water in the gas phase instead of the liquid (i.e., condensed) state that appears in living tissues, typically do not compare well with the available experimental data over the entire Bethe space. Moreover, first-principles simulations are cumbersome because of their high computational cost, particularly when dealing with a paradigmatic disordered system characterized by a large degree of amorphousness, such as liquid water. In principle, the computational complexity of calculating the ELF by time-dependent density functional theory (TDDFT) for all $\hbar k$ and E is largely due both to the size of the supercell necessary to describe its noncrystalline structure and the need to simulate a number of different molecular configurations to achieve the statistical significance of the averaged final result. However, to cut off the prohibitively expensive task of realizing an ensemble of statistically independent optimized water configurations, we limit our analysis to one particular cell configuration (32 water molecules at the experimental density in room conditions, ρ = 1 g/cm^3), assuming that the ELF is independent of the molecular configuration as shown in ref. 29 for its optical response. The Supporting Information details the procedure to generate a (periodic) water supercell as well as the methods for computing the electronic excitation spectrum. Figure 1 depicts the calculated ELF of liquid water compared to the available experimental data,[26−28] showing an excellent agreement in a wide range of energy and momentum transfers.

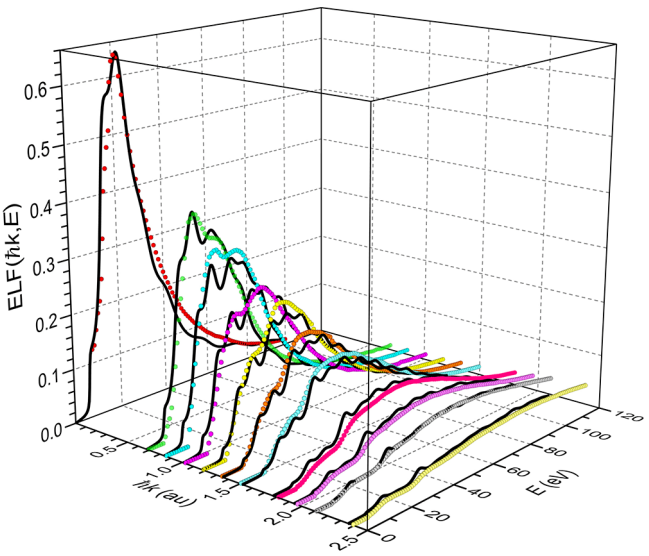

Figure 1. Energy-loss function (ELF) of liquid water as a function of the energy E and the momentum $\hbar k$ transfer. Black continuous curves represent TDDFT calculations, whereas symbols correspond to experimental data.[26−28]

The passage of swift charged particles through a medium prompts the generation of secondary electrons, which leads to subsequent cascade processes where these secondaries produce further electrons. All these charged particles lose energy and change their direction of motion by colliding with the medium constituents. It is currently admitted that the collision of secondary electrons with DNA from biological tissues can trigger irreparable damage if critical events, such as bond breaking of the nucleobase pairs or the sugar−phosphate chain, occur. The biodamage effectiveness increases when these episodes happen close enough (i.e., clustering) in the DNA molecule, as these events hamper the repair mechanisms.[13,30] The occurrence of these damaging events strongly depends on the energy with which the electrons reach the DNA molecule. Therefore, it is crucial to accurately know the characteristic energy range of the electrons reaching typical DNA volumes to better characterize the physical stage in radiation biodamage.

The main quantities for studying the generation, propagation, and effects of the secondary electrons produced by energetic ion beams in condensed phase media are the probability of ionization and the energy and angular distributions of the emitted electrons. These quantities are encoded in the inelastic scattering cross sections, which can be accurately calculated using the dielectric formalism[2,24,25] once the projectile (mass, charge, and energy) and medium (electronic excitation spectrum) characteristics are known. The procedure to obtain these cross sections is presented in the Supporting Information.

The doubly differential cross section (DDCS) for the angular distribution of electrons ejected with energy W per unit solid angle dΩ can be obtained from the ELF[31] using the procedure also described in the Supporting Information. This DDCS is depicted in Figure 2a together with available experimental measurements in the gas phase for carbon ions of the kinetic energy T = 6 MeV/u.[32] The agreement with the experimental data is fairly good for a wide range of electron energies W and angles θ, despite the phase differences between the calculations and the experiments. It is worth noting the

https://doi.org/10.1021/acs.jpclett.0c03250
J. Phys. Chem. Lett. 2021, 12, 487−493

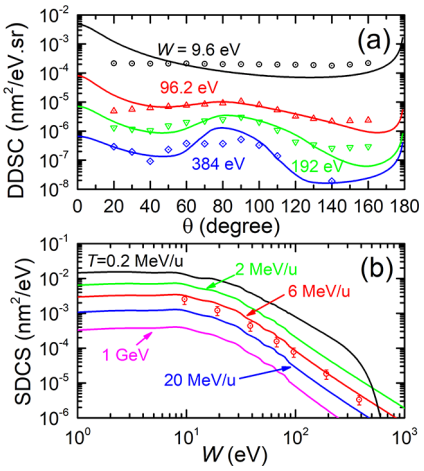

Figure 2. (a) Angular distribution of electrons with energy W generated by T = 6 MeV/u C ions in liquid water. (b) Energy distribution of electrons generated in liquid water by C ions with an initial kinetic energy T. Continuous lines represent our calculations, whereas symbols correspond to experimental data in water vapor.[32]

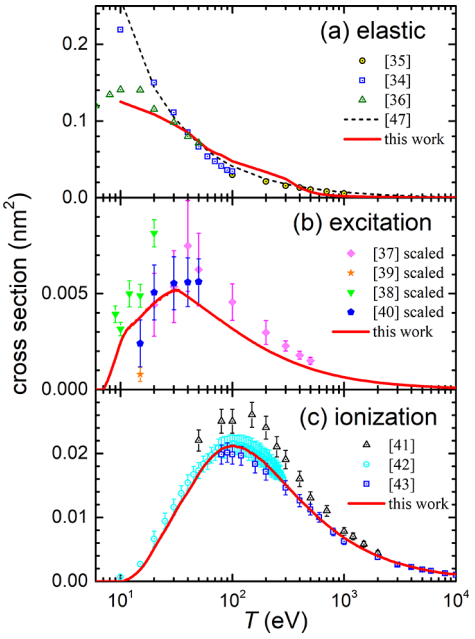

Figure 3. Cross sections of electrons in liquid water as a function of their energy W due to (a) elastic, (b) excitation, and (c) ionization processes. Curves correspond to calculations, as explained in the text. Symbols are experimental data for water vapor from (a) refs 34−36, (b) refs 37−40 (scaled), and (c) refs 41−43.

rather isotropic angular distribution of the lower-energy electrons.

The appropriate integration of the electronic excitation spectrum for all possible values of the momentum transfer $\hbar k$ provides the singly differential cross section (SDCS) of emission of electrons with energy W (see the Supporting Information). Figure 2b compares the calculated SDCS with the available experimental data for water vapor for several incident carbon-ion kinetic energies T from the typical values at the Bragg peak in hadrontherapy (0.2 MeV/u) to the very high ones appearing in cosmic radiation (1 GeV = 83.33 MeV/u). The comparison with measurements at T = 6 MeV/u[32] shows a good accordance, which is within the experimental error bars. Secondary-electron energy distributions are characterized by a peak at $W \simeq 10$ eV that rapidly decreases at higher energies. The SDCSs drop to zero at the maximum energy at which secondary electrons can be ejected. The abundance of low-energy electrons to which a significant role in clustered damage on the nanometer scale is attributed[12,18,33] is remarkable.

The energy transferred by the carbon ions to secondary electrons is carried away from the ion path as they propagate through the medium, where they undergo elastic collisions (leading to trajectory deviation) and inelastic interactions (resulting in electronic excitations, further ionizations, electron−phonon coupling, and trapping phenomena). Electron elastic scattering is reckoned with in this work by directly solving the Dirac−Hartree−Fock equation for a cluster of six water molecules to account for multiple scattering from the surrounding water molecules in the liquid phase by using a projected-potential approach[44,45] based on Gaussian functions[44−46] (see the Supporting Information for further details). In Figure 3a, we compare the elastic cross section we obtained using the water cluster (red curve) and the widely adopted Mott cross section[47] (dashed line). We stress the coincidence between the result obtained when using a single molecule in our Gaussian-based relativistic projected-potential approach and the Mott cross section, which is in excellent agreement with the recommended experimental data for water vapor (blue squares in Figure 3a).[34,35] At odds, Figure 3a clearly shows how the condensed-phase nature of liquid water emerges as a significant deviation from the single water molecule case (typically used in hadrontherapy modeling), particularly at low energies where the elastic cross section assessed on the cluster is appreciably reduced with respect to the single molecule; this behavior also appears in the experimental data by Cho et al.[36]

The main inelastic processes of electron projectiles (ionization and excitation of target electrons) are dealt with the dielectric formalism (see the Supporting Information) by replacing the ion characteristics with the electron ones as well as introducing indistinguishability and exchange. Upon the appropriate integration of the ELF for all $\hbar k$ and E transfers and properly accounting for excitation or ionization events,[48] the relevant cross sections were obtained. These are compared with experimental values available for a few specific excitation channels in the gas phase[37−40] (scaled to include all known channels)[49] and ionizations[41−43] in a broad energy range (10−10^4 eV) in Figure 3b and c, respectively. Despite the rather scattered experimental data, the excitation and ionization cross sections obtained from the ELF of liquid water exhibit a general shape and magnitude that is in fairly good agreement with the experimental results in the entire energy range. Remarkably, our calculations agree almost perfectly with the most recent experimental data.[42] Besides the previous inelastic processes, at energy $\lesssim$20 eV electrons may induce quasiparticle excitations (most notably phonons[50] and polarons[51]) or dissociative electron attachments.[18]

To reckon the electron transport within liquid water and the generation of the secondary electrons cascade, we used the event-by-event MC code SEED (secondary electron energy deposition),[52,53] which follows electron trajectories and accurately accounts for inelastic events (typically taking place at higher energy), resulting in the excitation and ionization of the medium atoms as well as elastic collisions with the atomic ions of the target (normally occurring below 50 eV) and

https://doi.org/10.1021/acs.jpclett.0c03250
J. Phys. Chem. Lett. 2021, 12, 487−493

leading to a change in trajectory when using the cross sections obtained above. Events particularly noticeable at low electron energies, such as electron−phonon and electron−polaron loss interactions as well as DEA processes, are also included in the simulation, as explained in the Supporting Information.

Indeed, it is the clustering of damaging events in nanometric volumes, mimicking the size of DNA, that determines biological effects, such as lethal lesions. Typically, these result in the clustered bond breaking of DNA molecules, a damage difficult to repair with the cell machinery that leads eventually to cell mutation or death.[11] Recently, the quantitative relation between the calculated complex DNA damage and the measured cell death probabilities was explicitly shown within the multiscale approach to the physics of radiation damage with ions.[13,23]

The physical processes that can lead to damage can be recorded by means of the SEED code.[52,53] The following damaging mechanisms were considered: (i) ionizations, (ii) electronic excitations leading to bond dissociation, and (iii) dissociative electron attachment events; the latter was simulated using the experimental cross section available for water molecules.[34,54,55] We assumed that only 40% of electronic excitation events lead to molecular dissociation[49] and thus produce damage. Figure 4 shows the average cluster

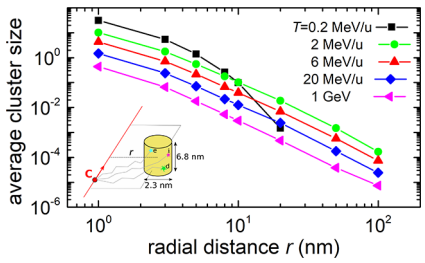

Figure 4. Average cluster size M_1 of damaging events in a sensitive volume of liquid water with a dimension of two DNA turns as a function of the radial distance r from the ion track for different values of the carbon-ion energy T. Symbols correspond to simulations, and lines are plotted to guide the eye. The inset depicts a scheme of the nanometric cylinder used in the scoring of the following damaging events: excitation (e), ionization (i), and dissociative electron attachment (d).

size M_1 of damaging events scored in nanometric cylinders of liquid water with a 2.3 nm diameter and a 6.8 nm height (see the inset in Figure 4), which is the size of 20 base pairs (bp) of DNA, for several carbon-ion energies T and impact parameters $0 \le r \le 100$ nm. To consider the inherently stochastic nature of the different interaction processes, a large number of ion shots at each ion kinetic energy were conducted (as explained in the Supporting Information), minimizing the statistical uncertainties so that the error bars in Figure 4 are smaller than the symbol size.

For 0.2 MeV/u ions, the average cluster sizes M_1 are significantly large ($\gtrsim 10$) at ion−target impact parameters $r <$ 3 nm and are always larger than 1 for $r < 5$ nm. The value of M_1 drops to 0 at $r > 20$ nm, meaning that secondary electrons cannot travel beyond that distance at this ion kinetic energy. Cluster-size distributions progressively decrease at increasing ion energies, although they are still larger than 1 at energies below 6 MeV/u with closer values of r (∼3−4 nm at 2 MeV/u and ∼2 nm at 6 MeV/u). The highest-energy (1 GeV) ions considered in this work are not capable of inducing clusters of average size ≥1 for any impact parameter. These trends show the potential of different ion kinetic energies to induce irreparable DNA damage; low-kinetic-energy ions around the Bragg peak region are especially harmful, producing large damage cluster sizes, while individual high-energy ions will not produce significant lethal damage.

From the cluster size distributions, it is possible to obtain useful statistical information on the probability of inducing complex DNA damage, which is the necessary information to relate the physical damage to biological outcomes. This is the purpose of experimental nanodosimetry,[20] which employs gas-phase detectors to estimate the probabilities of the clustering of inelastic events (estimated as ionizing collisions) in volumes of dimensions similar to those of sensitive nanometric DNA targets. Particularly important are the nanodosimetric quantities F_k (k = 1, 2, or 3), which indicate the cumulative probabilities of inducing clusters of a size $\ge k$ in a nanometric volume. F_2 is known to be correlated to the probability of inducing DNA double-strand breaks (DSB), while F_3 is connected to the probability of producing complex lethal damage.

Remarkably, it is known that the representation of the measured F_k^{ioniz} distributions for ionization events as a function of the average ionization cluster size M_1^{ioniz} yields a universal distribution independent of the size and characteristics of the particular nanodosimeter, which can be used to predict cell inactivation cross sections.[19,20] Our simulations provide these ionization distributions in nanometric cylinders of liquid water, which mimic DNA targets, at different values of the carbon-ion energy T and the impact parameter r. Figure 5 shows the plot

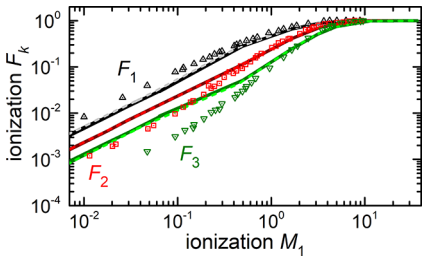

Figure 5. Simulation results of the ionization events F_k^{ioniz} (k = 1, 2, or 3) vs M_1^{ioniz} corresponding to several energies of the incident carbon ion and different impact parameters. Solid (dashed) lines correspond to a nanometric volume of 20 (10) base pairs. Symbols constitute a compilation of experimental data.[20]

F_k^{ioniz} (k = 1, 2, or 3) for ionization in the ranges 0.2 MeV/u to 1 GeV and $0 \le r \le 100$ nm as a function of the average ionization cluster size M_1^{ioniz}. Results are reported for the two target sizes relevant in evaluating lethal DNA damage, both of which have a diameter of 2.3 nm but a height of 3.4 or 6.8 nm that corresponds to DNA turns of 10 bp (dashed lines) or 20 bp (solid lines), respectively. Our simulations show a good agreement with nanodosimetric measurements in gas targets in a wide range of M_1^{ioniz} values,[20] confirming the universal relation F_k^{ioniz} vs M_1^{ioniz} for nanometric liquid water volumes. These data correspond to the impact parameters at which the largest amount of damaging events occur, i.e., for $r < 10$ nm for every ion energy. This result confirms the accuracy of both the simulations in liquid water and the nanodosimetric measurements in gas targets, and also shows that the relation F_k^{ioniz} vs

https://doi.org/10.1021/acs.jpclett.0c03250
J. Phys. Chem. Lett. 2021, 12, 487−493

M_1^{ioniz} scales irrespective of the size of the sensitive volume (10 bp or 20 bp DNA-like targets). Our F_k^{ioniz} distributions show a satisfactory behavior for the higher values of M_1^{ioniz} (corresponding to lower carbon energies or to the shorter impact parameters), although they deviate from experimental measurements at lower values (possibly due to differences between the gas and the liquid water targets at conditions where the number of damaging events is lower or to the electron−phonon and trapping cross sections). We stress the good agreement between the simulations and the experimental measurements of the ionization cluster size distribution, which is the only event experimentally measured.

We also used MC simulations, fed with accurate electronic excitation and ionization cross sections as well as the recommended dissociative electron attachment cross section for water,[34] to evaluate the specific contribution of each process to the average cluster sizes in a sensitive volume that had the dimensions of two DNA turns (i.e., 20 bp). These results are reported in Figure 6 for carbon-ion kinetic energies

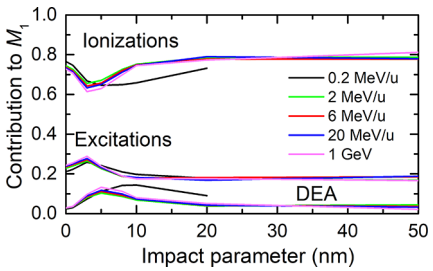

Figure 6. Fractional contribution to the average cluster size in a cylinder with a dimension of two DNA turns (20 bp) due to ionization, excitation (with only 40% of them leading to molecular dissociation), and dissociative electron attachments events for several carbon-ion kinetic energies and impact parameters.

in the range from 0.2 MeV/u to 1 GeV and impact parameters between the ion and the sensitive volume from 0 to 50 nm. The relative roles of the different damaging events (ionizations, excitations leading to molecular dissociation, and dissociative electron attachments) do not vary much neither with the carbon-ion kinetic energy nor with the impact parameter. This finding shows that ionizations contribute ∼80% to the average cluster size except at ∼5 nm impact parameters, where it is reduced to 60%. Electronic excitations leading to dissociation in general add up to ∼20% of the average cluster size at all kinetic energies, except for impact parameters around 5 nm where is ∼30%. However, dissociative electron attachments provide only 3% of the average cluster size at all kinetic energies and impact parameters; only at a very close impact parameter (∼5 nm) does its relative contribution amount to ∼10% of the total cluster size. For the lowest kinetic energy (0.2 MeV/u, matching the Bragg peak), the increased contribution of the dissociative electron attachment (15%) was observed at the 10 nm impact parameter at the expense of ionization. Note that this assessment relies on the assumption that only 40% of excitation events lead to bond breaking. In light of these results we can safely state that ionization events make up the vast majority of clustered damage mechanisms in liquid water (DNA-like) targets, which supports the use of ionization-based nanodosimeters.

In conclusion, we have presented an accurate description of the physical processes leading to the damage of living tissue (mimicked by liquid water medium) induced by swift carbon-ion beams in a wide energy range that addresses conditions typical of hadrontherapy and exposure to cosmic radiation. The main inelastic channels for charged particles, namely ionization and electronic excitation, were obtained from accurate TDDFT first-principles calculations of the electronic excitation spectrum (energy loss function, ELF) of liquid water, which via the dielectric formalism gave access to reliable inelastic cross sections to simulate the generation and propagation of secondary electrons abundantly produced by the energetic carbon-ion beam passing through the liquid water medium. *Ab initio* calculations of the elastic scattering cross section via a direct solution of the Dirac equation in water clusters to reproduce the condensed phase environment were also carried out, allowing precise MC simulations of the propagation of the (mostly) low-energy secondary electrons and their relevant effects at nanometer scale.

An analysis of the clustering of damaging events in nanometric volumes mimicking sensitive DNA targets was also conducted. This is important in the context of experimental nanodosimetry, relating cell response to the measurement of ionization clusters in gas-phase detectors.[19,20] The nature of damaging events (measurable ionizations vs other inelastic channels, namely dissociative excitations and dissociative electron attachments that are not accessible to nanodosimeters) and the effects of different phases (gas vs condensed) were investigated with unprecedented statistical accuracy.

We found that carbon ions with energy in proximity to the Bragg peak region, such as those typically used in hadrontherapy treatments, are capable of inducing large clusters of damaging events (>10 for ion-target distances $\lesssim$3 nm), while clusters tend to be much smaller for the larger energies. In particular, individual high-energy ions found in cosmic radiation are not capable of inducing average damage clusters larger than 1. We found that ∼70% of the events leading to the damaging cluster correspond to ionization processes. The obtained ionization cumulative distributions F_k^{ioniz}, represented as a function of the mean ionization cluster size M_1^{ioniz}, were found in excellent agreement with nanodosimetry measurements for the larger values of M_1^{ioniz} where most of the biological effects occur. These findings support the use of ionization-based detectors in nanodosimetry setups. Although a qualitative good agreement was found for the lower M_1^{ioniz} values, the presence of significant discrepancies requires deeper investigations. Nevertheless, we notice that a deviation for high-energy carbon ions may also arise due to the phase difference used in our simulations (liquid water) and that used in detectors (gas-phase).

Despite dissociative electron attachments being typically regarded as one of the most relevant biodamage mechanisms in radiotherapy, we found that our simulations point toward the limited role (∼10−15%) of dissociative electron attachment in carbon-ion-induced biodamage. Taking into account that only a fraction of dissociative electron attachments lead to irreversible damage,[56] we conclude that this process plays an almost negligible role in carbon-ion-induced biodamage; ionizations and excitations are the more significant physical processes resulting in harmful events due to carbon-ion irradiation in a wide energy range, covering those relevant to hadrontherapy up to those from cosmic radiation.

https://doi.org/10.1021/acs.jpclett.0c03250
J. Phys. Chem. Lett. 2021, 12, 487−493

■ ASSOCIATED CONTENT

Supporting Information

The Supporting Information is available free of charge at https://pubs.acs.org/doi/10.1021/acs.jpclett.0c03250.

Theoretical and computational procedures for (i) the assessment of the ELF of liquid water; (ii) cross sections of inelastic and elastic events; and (iii) the generation, transport, and effects of secondary electrons (PDF)

■ AUTHOR INFORMATION

Corresponding Authors

Simone Taioli − *European Centre for Theoretical Studies in Nuclear Physics and Related Areas (ECT*-FBK) and Trento Institute for Fundamental Physics and Applications (TIFPA-INFN), 38123 Trento, Italy; Peter the Great St. Petersburg Polytechnic University, 195251 Saint Petersburg, Russia;* orcid.org/0000-0003-4010-8000; Email: taioli@ectstar.eu

Maurizio Dapor − *European Centre for Theoretical Studies in Nuclear Physics and Related Areas (ECT*-FBK) and Trento Institute for Fundamental Physics and Applications (TIFPA-INFN), 38123 Trento, Italy;* orcid.org/0000-0001-6855-0189; Email: dapor@ectstar.eu

Authors

Paolo E. Trevisanutto − *European Centre for Theoretical Studies in Nuclear Physics and Related Areas (ECT*-FBK) and Trento Institute for Fundamental Physics and Applications (TIFPA-INFN), 38123 Trento, Italy; Center for Information Technology, Bruno Kessler Foundation, 38123 Trento, Italy*

Pablo de Vera − *European Centre for Theoretical Studies in Nuclear Physics and Related Areas (ECT*-FBK) and Trento Institute for Fundamental Physics and Applications (TIFPA-INFN), 38123 Trento, Italy; Departamento de Física, Centro de Investigación en Óptica y Nanofísica, Universidad de Murcia, 30100 Murcia, Spain;* orcid.org/0000-0002-5645-412X

Stefano Simonucci − *School of Science and Technology, University of Camerino, 62032 Camerino, Italy; INFN, Sezione di Perugia, 06123 Perugia, Italy*

Isabel Abril − *Departament de Física Aplicada, Universitat d'Alacant, 03080 Alacant, Spain*

Rafael Garcia-Molina − *Departamento de Física, Centro de Investigación en Óptica y Nanofísica, Universidad de Murcia, 30100 Murcia, Spain;* orcid.org/0000-0001-8755-8709

Complete contact information is available at: https://pubs.acs.org/10.1021/acs.jpclett.0c03250

Notes

The authors declare no competing financial interest.

■ ACKNOWLEDGMENTS

M.D. and S.T. acknowledge the Bruno Kessler Foundation and the National Institute of Nuclear Physics for unlimited access to their computing facilities, and the Caritro Foundation for the grant High-Z ceramic oxide nanosystems for mediated proton cancer therapy. This project received funding from the European Union's Horizon 2020 Research and Innovation programme under the Marie Sklodowska-Curie grant agreement no. 840752. P.d.V. received additional support by the Spanish Ministerio de Ciencia e Innovación by means of a Juan de la Cierva fellowship (no. FJCI-2017-32233). This work was also supported by the Spanish Ministerio de Ciencia e Innovación and the European Regional Development Fund (Project PGC2018-096788−B−I00); the Fundación Séneca−Agencia de Ciencia y Tecnología de la Región de Murcia (Project 19907/GERM/15); and the Conselleria d'Educació, Investigació, Cultura i Esport de la Generalitat Valenciana (Project AICO/2019/070).

■ REFERENCES

(1) Nastasi, M. A.; Mayer, J. W.; Hirvonen, J. K. *Ion-Solid Interactions: Fundamentals and Applications*; Clarke, D. R., Suresh, S., Ward, I. M., Eds.; Cambridge Solid State Science Series, Vol. *151*; Cambridge University Press: Cambridge, U.K., 1996.

(2) Nikjoo, H.; Uehara, S.; Emfietzoglou, D. *Interaction of Radiation with Matter*; CRC Press: Boca Raton, FL, 2012.

(3) Imaging in Medical Diagnosis and Therapy. In *Proton and Carbon Ion Therapy*; Ma, C.-M. C. M., Lomax, T., Eds.; CRC Press: Boca Raton, FL, 2013.

(4) Surdutovich, E.; Solov'yov, A. V. Multiscale approach to the physics of radiation damage with ions. *Eur. Phys. J. D* **2014**, *68*, 353.

(5) Suit, H.; Delaney, T. F.; Trofimov, A. Physical and Biological Basis of Proton and of Carbon Ion Radiation Therapy and Clinical Outcome Data. In *Medical Applications of Accelerators*; Chao, A. W., Chou, W., Eds.; Reviews of Accelerator Science and Technology, Vol. *II*; World Scientific: Singapore, 2009; pp 1−15.

(6) Amaldi, U.; Bonomi, R.; Braccini, S.; Crescenti, M.; Degiovanni, A.; Garlasche, M.; Garonna, A.; Magrin, G.; Mellace, C.; Pearce, P.; et al. Accelerators for hadrontherapy: From Lawrence cyclotrons to linacs. *Nucl. Instrum. Methods Phys. Res., Sect. A* **2010**, *620*, 563−577.

(7) Ebner, D. K.; Kamada, T. The Emerging Role of Carbon-Ion Radiotherapy. *Front. Oncol.* **2016**, *6*, 140.

(8) Durante, M.; Cucinotta, F. A. Physical basis of radiation protection in space travel. *Rev. Mod. Phys.* **2011**, *83*, 1245−1281.

(9) Vignoli Muniz, G. S.; Mejía, C. F.; Martinez, R.; Auge, B.; Rothard, H.; Domaracka, A.; Boduch, P. Radioresistance of Adenine to Cosmic Rays. *Astrobiology* **2017**, *17*, 298−308.

(10) Vepsäläinen, A. P.; Karamlou, A. H.; Orrell, J. L.; Dogra, A. S.; Loer, B.; Vasconcelos, F.; Kim, D. K.; Melville, A. J.; Niedzielski, B. M.; Yoder, J. L.; et al. Impact of ionizing radiation on superconducting qubit coherence. *Nature* **2020**, *584*, 551−556.

(11) Goodhead, D. T. Initial events in the cellular effects of ionizing radiations: clustered damage in DNA. *Int. J. Radiat. Biol.* **1994**, *65*, 7−17.

(12) Alizadeh, E.; Orlando, T. M.; Sanche, L. Biomolecular Damage Induced by Ionizing Radiation: The Direct and Indirect Effects of Low-Energy Electrons on DNA. *Annu. Rev. Phys. Chem.* **2015**, *66*, 379−398.

(13) Verkhovtsev, A.; Surdutovich, E.; Solov'yov, A. V. Multiscale approach predictions for biological outcomes in ion-beam cancer therapy. *Sci. Rep.* **2016**, *6*, 27654.

(14) *Charged Particle and Photon Interactions with Matter: Chemical, Physicochemical, and Biological Consequences with Applications*; Mozumder, A., Hatano, Y., Eds.; Marcel Dekker, Inc.: New York, NY, 2004.

(15) *Nanoscale Insights into Ion-Beam Cancer Therapy*; Solov'yov, A. V., Ed.; Springer International Publishing: Cham, Switzerland, 2017.

(16) Baldacchino, G.; Brun, E.; Denden, I.; Bouhadoun, S.; Roux, R.; Khodja, H.; Sicard-Roselli, C. Importance of radiolytic reactions during high-LET irradiation modalities: LET effect, role of O_2 and radiosensitization by nanoparticles. *Cancer Nanotechnol.* **2019**, *10*, 3.

(17) Hirayama, R.; Ito, A.; Tomita, M.; Tsukada, T.; Yatagai, F.; Matsumoto, Y.; Kase, Y.; Ando, K.; Okayasu, R.; Furusawa, Y.; et al. Contributions of Direct and Indirect Actions in Cell Killing by High-LET Radiations. *Radiat. Res.* **2009**, *171*, 212−218.

(18) Boudaïffa, B.; Cloutier, P.; Hunting, D.; Huels, M. A.; Sanche, L. Resonant Formation of DNA Strand Breaks by Low-Energy (3 to 20 eV) Electrons. *Science* **2000**, *287*, 1658−1660.

(19) Conte, V.; Selva, A.; Colautti, P.; Hilgers, G.; Rabus, H. Track structure characterization and its link to radiobiology. *Radiat. Meas.* **2017**, *106*, 506−511.
(20) Conte, V.; Selva, A.; Colautti, P.; Hilgers, G.; Rabus, H.; Bantsar, A.; Pietrzak, M.; Pszona, S. Nanodosimetry: Towards a New Concept of Radiation Quality. *Radiat. Prot. Dosim.* **2018**, *180*, 150−156.
(21) Solov'yov, A.; Surdutovich, E.; Scifoni, E.; Mishustin, I.; Greiner, W. Physics of ion beam cancer therapy: A multiscale approach. *Phys. Rev. E* **2009**, *79*, 011909.
(22) Surdutovich, E.; Solov'yov, A. V. Transport of secondary electrons and reactive species in ion tracks. *Eur. Phys. J. D* **2015**, *69*, 193.
(23) Surdutovich, E.; Solov'yov, A. V. Multiscale modeling for cancer radiotherapies. *Cancer Nanotechnol.* **2019**, *10*, 6.
(24) Lindhard, J. On the properties of a gas of charged particles. *Dan. Mater. Fys. Medd.* **1954**, *28* (8), 1−57.
(25) Ritchie, R. H. Interaction of charged particles with a degenerate Fermi−Dirac electron gas. *Phys. Rev.* **1959**, *114*, 644−654.
(26) Watanabe, N.; Hayashi, H.; Udagawa, Y. Bethe surface of liquid water determined by inelastic X-ray scattering spectroscopy and electron correlation effects. *Bull. Chem. Soc. Jpn.* **1997**, *70*, 719−726.
(27) Hayashi, H.; Watanabe, N.; Udagawa, Y.; Kao, C. The complete optical spectrum of liquid water measured by inelastic x-ray scattering. *Proc. Natl. Acad. Sci. U. S. A.* **2000**, *97*, 6264−6266.
(28) Watanabe, N.; Hayashi, H.; Udagawa, Y. Inelastic X-ray scattering study on molecular liquids. *J. Phys. Chem. Solids* **2000**, *61*, 407−409.
(29) Garbuio, V.; Cascella, M.; Reining, L.; Sole, R. D.; Pulci, O. Ab Initio Calculation of Optical Spectra of Liquids: Many-Body Effects in the Electronic Excitations of Water. *Phys. Rev. Lett.* **2006**, *97*, 137402.
(30) Nikjoo, H.; Emfietzoglou, D.; Liamsuwan, T.; Taleei, R.; Liljequist, D.; Uehara, S. Radiation track, DNA damage and response — a review. *Rep. Prog. Phys.* **2016**, *79*, 116601.
(31) de Vera, P.; Garcia-Molina, R.; Abril, I. Angular and Energy Distributions of Electrons Produced in Arbitrary Biomaterials by Proton Impact. *Phys. Rev. Lett.* **2015**, *114*, 018101.
(32) Dal Cappello, C.; Champion, C.; Boudrioua, O.; Lekadir, H.; Sato, Y.; Ohsawa, D. Theoretical and experimental investigations of electron emission in C^{6+} + H_2O collisions. *Nucl. Instrum. Methods Phys. Res., Sect. B* **2009**, *267*, 781−790.
(33) Rezaee, M.; Hunting, D.; Sanche, L. Correlation between energy deposition and molecular damage from Auger electrons: A case study of ultra-low energy (5−18 eV) electron interactions with DNA. *Med. Phys.* **2014**, *41*, 072502.
(34) Itikawa, Y.; Mason, N. Cross Sections for Electron Collisions with Water Molecules. *J. Phys. Chem. Ref. Data* **2005**, *34*, 1−22.
(35) Katase, A.; Ishibashi, K.; Matsumoto, Y.; Sakae, T.; Maezono, S.; Murakami, E.; Watanabe, K.; Maki, H. Elastic scattering of electrons by water molecules over the range 100−1000 eV. *J. Phys. B: At. Mol. Phys.* **1986**, *19*, 2715−2734.
(36) Cho, H.; Park, Y. S.; Tanaka, H.; Buckman, S. J. Measurements of elastic electron scattering by water vapour extended to backward angles. *J. Phys. B: At., Mol. Opt. Phys.* **2004**, *37*, 625−634.
(37) Thorn, P. A.; Brunger, M. J.; Teubner, P. J. O.; Diakomichalis, N.; Maddern, T.; Bolorizadeh, M. A.; Newell, W. R.; Kato, H.; Hoshino, M.; Tanaka, H.; et al. Cross sections and oscillator strengths for electron-impact excitation of the $\tilde{A}\ ^1B_1$ electronic state of water. *J. Chem. Phys.* **2007**, *126*, 064306.
(38) Ralphs, K.; Serna, G.; Hargreaves, L. R.; Khakoo, M. A.; Winstead, C.; McKoy, V. Excitation of the six lowest electronic transitions in water by 9−20 eV electrons. *J. Phys. B: At., Mol. Opt. Phys.* **2013**, *46*, 125201.
(39) Brunger, M. J.; Thorn, P. A.; Campbell, L.; Diakomichalis, N.; Kato, H.; Kawahara, H.; Hoshino, M.; Tanaka, H.; Kim, Y.-K. Excitation of the lowest lying 3B1, 1B1, 3A2, 1A2, 3A1 and 1A1 electronic states in water by 15 eV electrons. *Int. J. Mass Spectrom.* **2008**, *271*, 80−84.
(40) Matsui, M.; Hoshino, M.; Kato, H.; da Silva, F. F.; Limão-Vieira, P.; Tanaka, H. Measuring electron-impact cross sections of water: elastic scattering and electronic excitation of the $\tilde{a}^3B_1$ and $\tilde{A}^1B_1$ states. *Eur. Phys. J. D* **2016**, *70*, 77.
(41) Bolorizadeh, M. A.; Rudd, M. E. Angular and Energy Dependence of Cross Sections for Ejection of Electrons from Water Vapor. I. 50−2000-eV Electron Impact. *Phys. Rev. A: At., Mol., Opt. Phys.* **1986**, *33*, 882−887.
(42) Bull, J. N.; Lee, J. W. L.; Vallance, C. Absolute electron total ionization cross-sections: molecular analogues of DNA and RNA nucleobase and sugar constituents. *Phys. Chem. Chem. Phys.* **2014**, *16*, 10743−10752.
(43) Schutten, J.; de Heer, F. J.; Moustafa, H. R.; Boerboom, A. J. H.; Kistemaker, J. Cross- and Partial-Ionization Cross Sections for Electrons on Water Vapor in the Energy Range 0.1−20 keV. *J. Chem. Phys.* **1966**, *44*, 3924−3928.
(44) Taioli, S.; Simonucci, S.; Calliari, L.; Dapor, M. Electron spectroscopies and inelastic processes in nanoclusters and solids: Theory and experiment. *Phys. Rep.* **2010**, *493*, 237−319.
(45) Taioli, S.; Simonucci, S.; Dapor, M. SURPRISES: when ab initio meets statistics in extended systems. *Comput. Sci. Discovery* **2009**, *2*, 015002.
(46) Morresi, T.; Taioli, S.; Simonucci, S. Nuclear Beta Decay: Relativistic Theory and Ab Initio Simulations of Electroweak Decay Spectra in Medium-Heavy Nuclei and of Atomic and Molecular Electronic Structure. *Advanced Theory and Simulations* **2018**, *1*, 1870030.
(47) Mott, N. F. The scattering of fast electrons by atomic nuclei. *Proc. R. Soc. London A* **1929**, *124* (794), 425−442.
(48) de Vera, P.; Garcia-Molina, R. Electron Inelastic Mean Free Paths in Condensed Matter Down to a Few Electronvolts. *J. Phys. Chem. C* **2019**, *123*, 2075−2083.
(49) Thorn, P. A. *Electronic State Excitations in the Water Molecule by Collisions with Low Energy Electrons*. Ph.D. Thesis, Flinders University of South Australia, Adelaide, Australia, 2008.
(50) Fröhlich, H. Electrons in lattice fields. *Adv. Phys.* **1954**, *3*, 325−361.
(51) Ganachaud, J.; Mokrani, A. Theoretical study of the secondary electron emission of insulating targets. *Surf. Sci.* **1995**, *334*, 329−341.
(52) Dapor, M.; Abril, I.; de Vera, P.; Garcia-Molina, R. Energy deposition around swift proton tracks in polymethylmethacrylate: How much and how far. *Phys. Rev. B: Condens. Matter Mater. Phys.* **2017**, *96*, 064113.
(53) Dapor, M. *Transport of Energetic Electrons in Solids. Computer Simulation with Applications to Materials Analysis and Characterization*, 3rd ed.; Springer Nature: Cham, Switzerland, 2020.
(54) Taioli, S.; Tennyson, J. A wave packet method for treating nuclear dynamics on complex potentials. *J. Phys. B: At., Mol. Opt. Phys.* **2006**, *39*, 4379−4392.
(55) Taioli, S.; Tennyson, J. WATERWAVES: wave particles dynamics on a complex triatomic potential. *Comput. Phys. Commun.* **2006**, *175*, 41−51.
(56) Kohanoff, J.; McAllister, M.; Tribello, G. A.; Gu, B. Interactions between low energy electrons and DNA: a perspective from first-principles simulations. *J. Phys.: Condens. Matter* **2017**, *29*, 383001.

NOTE ADDED AFTER ISSUE PUBLICATION

This article was initially published with an incorrect copyright statement and was corrected on or around May 5, 2021.

https://doi.org/10.1021/acs.jpclett.0c03250
J. Phys. Chem. Lett. 2021, 12, 487−493